Turkish Journal of Electrical Engineering & Computer Sciences

http://journals.tubitak.gov.tr/elektrik/

Research Article

Turk J Elec Eng & Comp Sci
(2014) 22: 1 – 11

doi:10.3906/elk-1204-94

A performance comparison of linear and nonlinear control of a SCIG-wind farm connecting to a distribution network

Mohamed BENCHAGRA[1,*], **Mohamed MAAROUFI**[1], **Mohammed OUASSAID**[2]

[1]Department of Electrical Engineering, Mohammadia School of Engineering, University Mohammed V-Agdal, Rabat, Morocco

[2]Department of Industrial Engineering, National School of Application Sciences, Cadi Ayyad University, Morocco

Received: 30.04.2012 • **Accepted:** 15.10.2012 • **Published Online:** 20.12.2013 • **Printed:** 20.01.2014

Abstract: This study presents a comparison of linear and nonlinear control to regulate the DC-link voltage and power factor correction of a wind farm equipped with squirrel cage induction generators (SCIGs), connecting to a 22-kV distribution network. Both active and reactive powers are employed in 2 independent control laws. The proposed control strategies are derived from the Lyapunov approach. The aim of the control is to maximize the generated power with the lowest possible impact in the grid voltage and frequency during normal operation and under the occurrence of faults. The nonlinear backstepping controller to be used for the control of the designed system is studied and compared with a classical proportional-integral controller for performance validation. The entire designed system is modeled and simulated using MATLAB/Simulink.

Key words: Renewable energy, wind farm, squirrel cage induction generator, DC-link voltage control, power factor correction control, nonlinear control, backstepping approach, distribution network

1. Wind farm connected distribution network

When large renewable energy sources are integrated into a distribution network, the dynamics and the operations of the network are affected [1]. The emergence of the smart grid will pose wind turbine (WT) developers with a new challenge: production during high wind speed, the value of the total harmonic distortion (THD), and power factor correction (PFC). The WT should be able to continuously supply the network. Among the technology choices, squirrel cage induction generators (SCIGs) are a very attractive choice for wind power generation because they are robust, inexpensive, and have low maintenance requirements and costs. As a network interface, the use of a back-to-back converter for speed operation is extensively reported in the literature, showing their capability to achieve maximum energy capture in a wide range of wind conditions [2–4].

This renewable system generation has many uncertainties due to the erratic nature of wind-based systems. Therefore, the controller should accommodate the effects of uncertainties, keep the system stable against a large variation of wind speed, and produce good power quality. The conventional proportional-integral (PI) controller cannot fully satisfy stability and performance requirements. On the other hand, the wind power system is a highly nonlinear system and has a large range of operating points. Thus, linearization around one operating point cannot be employed to design the controllers. In this case, a nonlinear control method can be used to effectively solve this problem.

*Correspondence: m.benchagra@gmail.com

In the literature, different controlling types of wind energy sources and power electronic converters can be seen. In some research, control techniques such as PI control [5–8], fuzzy logic control [2], and fuzzy neural networks [9,10] are frequently used. In an attempt to achieve high performances in the steady state as well as during the transient state, the nonlinear control structure must be applied. In the last 2 decades, many modified nonlinear state feedback controls, such as input-output feedback linearization control, based on the sliding mode approach, were applied to improve power system control performances [11]. Specifically during these years, there was a tremendous amount of activity on special control schemes known as 'backstepping' approaches. The backstepping approach is a nonlinear method that is perfectly suited for power generation connected power networks [12].

This paper focuses on nonlinear backstepping control (NBC) combined with a SCIG-WT interfaced to the distribution system with back-to-back converter model. The fixing of the DC-link voltage amplitude at a constant value, such as 760 V, and PFC using a NBC is elaborated and explained. The wind velocity is continuously changed and the behavior of the system is analyzed. For the controllers, both a PI controller and a NBC are used, and the results are compared. The value of the THD and the voltage hold at the standard intervals. The entire system and all of its subcomponents are designed in a MATLAB/Simulink/SPS environment.

2. Wind farm connected distribution network

2.1. System configuration

The schematic diagram of the studied wind farm based on a SCIG-connected distribution network is shown in Figure 1. All of the subsystem components [WT, voltage source inverter (VSI), PI controller, nonlinear controller, filter, transformer, and distribution system] are submodeled individually using the MATLAB environment and combined to establish the overall system model. The simulation of the proposed scheme is done in a MATLAB/Simulink/SPS environment to establish the model validation and component compatibility.

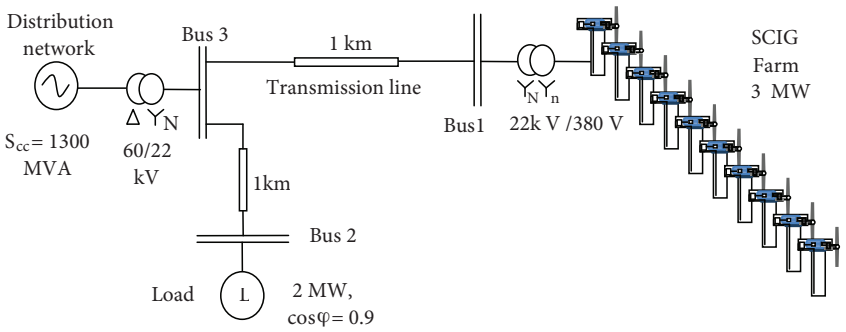

Figure 1. Schematic representation of the system.

The schematic diagram of the studied WT based on a SCIG is shown in Figure 2. The turbine rotor shaft of the studied SCIG is coupled to the hub of the turbine through a gearbox for transforming the low rotational speeds of the turbine to the required higher rotational speeds of the SCIG. The mechanical energy is transformed into electrical energy by the generator, and the back-to-back electronic converter is the interface between the generator and the distribution network. The NBC provides proper switching signals for the voltage source converter (VSC) SCIG-side so as to extract the maximum power from the WT [13]. The output of the controller is used to generate a pulse-width modulation (PWM) signal, which is used to control the output

voltage of the VSI distribution network-side. The frequency of the VSI is controlled and maintained at 50 Hz through a phase-locked loop (PLL) process.

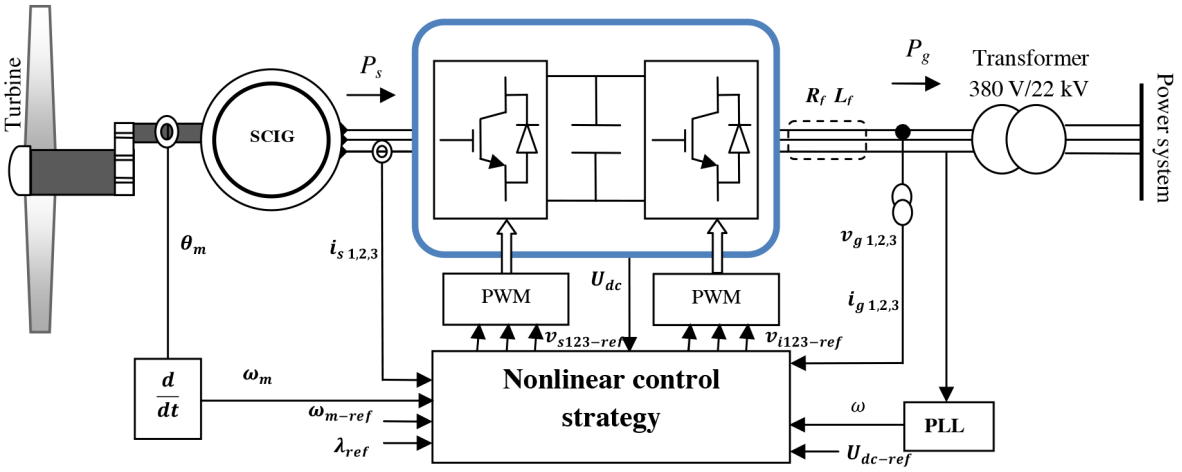

Figure 2. The overall diagram of the proposed control.

In this study, a wind farm system supplying power to a 3-phase distributed system is examined. To fix the voltage on the DC-bus at 760 V and frequency to 50 Hz on the VSI, both PI controllers and NBCs are used and the results are compared.

2.2. The wind turbine and pitch control model

WTs convert mechanical energy produced by the wind to electrical energy. The model of the WT and pitch control is developed on the basis of the turbine's steady-state power characteristics.

The mechanical torque produced by the WT is given by:

$$T_m = \frac{\rho \pi R^2}{2\Omega_t} v^3 C_p(\beta\delta), \tag{1}$$

where ρ is the air density, R is the radius of the turbine, and v is the wind velocity. $C_p(\delta,\beta)$ is the power coefficient and Ω_t is the turbine speed, which is a function of mechanical speed ω_m and gear ratio G ($\Omega_t = \omega_m / G$). β is the rotor blade pitch angle and $\delta = \Omega_t R/v$ is the tip-speed ratio.

We consider a generic equation to model the power coefficient C_p, based on the modeling turbine characteristics described in [14]:

$$\begin{aligned} C_p(\delta,\beta) &= 0.5109\left(\tfrac{116}{\delta_i} - 0.4\beta - 5\right)\exp\left(\tfrac{-21}{\delta_i}\right) \\ \delta_i &= -\left[\tfrac{1}{(\delta+0.08\beta)} - \tfrac{0.035}{(\beta^3+1)}\right]^{-1}. \end{aligned} \tag{2}$$

Because the maximum $C_p(\delta,\beta)$ is obtained at optimal tip-speed ratio $\delta = \delta_{opt}$, looking to take the maximum power available at any wind speed, the control system must adjust the mechanical speed to operate at δ_{opt}. A relationship between C_p and δ for various values of the pitch angle β is illustrated in Figure 3. The maximum value of C_p, i.e. $C_{pmax} = 0.47$, is achieved for $\beta = 0°$ and $\delta_{opt} = 8.1$.

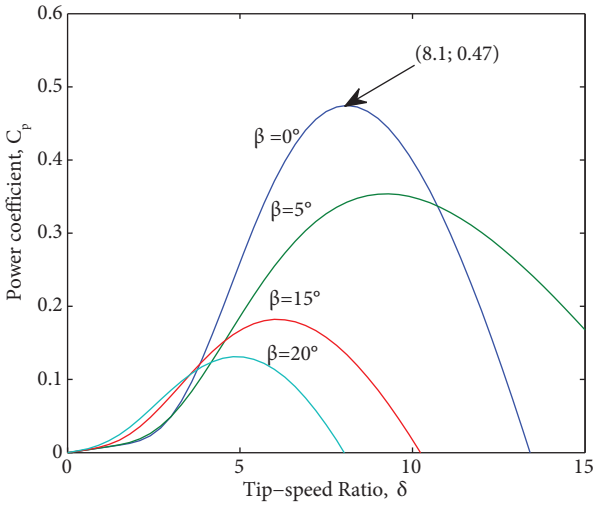

Figure 3. Characteristics C_p vs. δ for the various values of pitch angle β.

3. Nonlinear control of the SCIG-connected distribution network

3.1. Nonlinear model of the SCIG

The model of the studied SCIG can be written as:

$$\frac{di_{ds}}{dt} = -a_1 i_{ds} + \omega_s i_{qs} + a_2 \lambda_{dr} + a_3 \omega_m \lambda_{qr} + a_4 v_{ds}, \tag{3}$$

$$\frac{di_{qs}}{dt} = -a_1 i_{qs} - \omega_s i_{ds} + a_2 \lambda_{qr} - a_3 \omega_m \lambda_{dr} + a_4 v_{qs}, \tag{4}$$

$$\frac{d\lambda_{dr}}{dt} = a_5 i_{ds} - a_6 \lambda_{dr} + (\omega_s - p\omega_m)\lambda_{qr}, \tag{5}$$

$$\frac{d\lambda_{qr}}{dt} = a_5 i_{qs} - a_6 \lambda_{qr} - (\omega_s - p\omega_m)\lambda_{dr}, \tag{6}$$

$$\frac{d\omega_m}{dt} = a_7 \left(\lambda_{dr} i_{qs} - \lambda_{qr} i_{ds}\right) - a_8 \omega_m - a_9 T_m, \tag{7}$$

where $a_1 = \left(L_r^2 R_s + L_m^2 R_r\right) / \sigma L_s L_r^2$;$a_2 = R_r L_m / \sigma L_s L_r^2$; $a_3 = pR_r / \sigma L_s L_r$;$a_4 = 1 / \sigma L_s$; $a_5 = R_r L_m / L_r$; $a_6 = R_r / L_r$; $a_7 = pL_m / JL_r$; $a_8 = f / J$; $a_9 = 1 / J$.

Here, i_{ds} and i_{qs} are the d-axis and q-axis stator currents, respectively; v_{ds} and v_{qs} are the d-axis and q-axis stator voltages; λ_{dr} and λ_{qr} are the d-axis and q-axis rotor fluxes; ω_m is the mechanical speed; ω_s is the electrical angular speed of the SCIG; and T_m is the mechanical torque.

From the presented model it is seen that the SCIG is a nonlinear multivariable system with coupling between the direct and quadrate axes. This model is dependent on the stator electrical speed ω_s, and this variable can be calculated if the dq reference frame is synchronized with the rotor flux. Fixing the d-axis of the rotating reference frame on the rotor flux vector, we have $\lambda_{dr} = \lambda_r$ and $\lambda_{qr} = 0$.

In this case, 2 state variables are proposed for describing the SCIG model in order to extract the maximum power from the turbine, mechanical speed, and rotor flux:

$$\dot{\omega}_m = a_7 \lambda_{dr} i_{qs} - a_8 \omega_m - a_9 T_m, \tag{8}$$

$$\dot{\lambda}_{dr} = a_5 i_{ds} - a_6 \lambda_{dr}. \tag{9}$$

3.2. Nonlinear control strategy of the DC-link voltage and PFC

The basic idea of the backstepping design is the use of the 'virtual control' states to decompose systematically a complex nonlinear control structure problem into simpler and smaller ones. The backstepping design is divided into 2 various steps. In each one, we deal with an easier single-input, single-output problem and each step provides a reference for the next step [15].

The aim of the VSI is to regulate the DC-link voltage and maintain the balance between the DC-link power and the power supplied to the distribution network. This is done by actively controlling the direct axis current component of the converter. To do that, the VSI 3-phase currents and voltages are expressed in 2 axis reference frames, synchronously rotating at the distribution network frequency, and so $v_{qg} = 0$. In this case, the DC-link voltage can be controlled by modulating the converter direct axis current component i_{dg} when the VSI quadrate current component i_{qg} is used to modulate the flow of reactive power.

The d- and q-axis voltages, current, and DC-link voltage equations of the VSI-side transmission line are given by:

$$\frac{di_{dg}}{dt} = -b_1 i_{dg} + b_2 i_{qg} + b_3(v_{di} - v_{dg}), \tag{10}$$

$$\frac{di_{qg}}{dt} = -b_1 i_{qg} - b_2 i_{dg} + b_3 v_{qi}, \tag{11}$$

$$\frac{dU_{dc}^2}{dt} = \frac{2}{C}(-\frac{3}{2} v_{dg} i_{dg} + P_s), \tag{12}$$

where $b_1 = R_t/L_t$, $b_2 = \omega$, and $b_3 = 1 \ / \ L_t$. R_t and L_t are the resistance and inductance of the filter, respectively; ω is the distribution network frequency; and P_s is the power supplied by the generator.

From Eq. (13), it is clear that the DC-link voltage controller provides the active power reference value (or direct current reference i_{dg-ref}) and P_s acts as a disturbance.

We turn to the backstepping design steps. First, for the DC-link voltage regulation tracking objective, we define the error as:

$$e_{U_{dc}^2} = U_{dc-ref}^2 - U_{dc}^2. \tag{13}$$

Next, the error dynamical equation is:

$$\dot{e}_{U_{dc}^2} = \dot{U}_{dc-ref}^2 - \frac{2}{C}\left(-\frac{3}{2} v_{dg} i_{dg}^* + P_s\right). \tag{14}$$

Since the objective requires that the error converge to 0, we could satisfy the objective by viewing i_{dg} as a virtual control variable in the above equation and use it to control the error $e_{U_{dc}^2}$.

The Lyapunov function is defined by:

$$V_{U_{dc}^2} = \frac{1}{2} e_{U_{dc}^2}^2. \tag{15}$$

The derivative of $V_{U_{dc}^2}$ along the error equation is:

$$\begin{aligned} \dot{V}_{U_{dc}^2} &= \dot{e}_{U_{dc}^2} e_{U_{dc}^2} = e_{U_{dc}^2}\left(\dot{U}_{dc-ref}^2 - \tfrac{2}{C}\left(-\tfrac{3}{2} v_{dg} i_{dg}^* + P_s\right)\right) \\ &= k_{U_{dc}^2} e_{U_{dc}^2}^2 + e_{U_{dc}^2}\left(\dot{U}_{dc-ref}^2 - \tfrac{2}{c}\left(-\tfrac{3}{2} v_{dg} i_{dg}^* + P_s\right) + k_{U_{dc}^2} e_{U_{dc}^2}\right), \end{aligned} \tag{16}$$

where $k_{U_{dc}^2}$ is a positive design constant that determines the closed-loop dynamic. Thus, the tracking objective will be satisfied if we choose the stabilizing function as:

$$i_{dg}^* = \frac{1}{v_{dg}} \left(\frac{2}{3} P_s - \frac{C}{3} \left(\dot{U}_{dc-ref}^2 + k_{U_{dc}^2} e_{U_{dc}^2} \right) \right), \tag{17}$$

since the choice of Eq. (18) gives:

$$\dot{V}_{U_{dc}^2} = -k_{U_{dc}^2} e_{U_{dc}^2}^2 \leq 0. \tag{18}$$

Eq. (18) indicates that the virtual control should be in order to satisfy the control objective of active power, so it provides the reference for the next step and tries to make signal i_{dg} behave as desired. Hence, we define again the error signals involving the desired variables, i_{dg} and i_{qg} ($i_{qg-ref} = i_{qg}^*$), in order to control the active and reactive powers, respectively:

$$e_{idg} = i_{dg}^* - i_{dg}, \tag{19}$$

$$e_{iqg} = i_{qg}^* - i_{qg}. \tag{20}$$

Next, the error equation in Eq. (15) can be expressed as:

$$\dot{e}_{U_{dc}^2} = -k_{U_{dc}^2} e_{U_{dc}^2} + \frac{3}{C} v_{dg}\, e_{i_{dg}}. \tag{21}$$

Moreover, the dynamical equations for the error signals, e_{idg} and e_{iqg}, can be computed as:

$$\dot{e}_{idg} = \frac{di_{dg}^*}{dt} - \left(-b_1 i_{dg} + b_2 i_{qg} + b_3 (v_{di} - v_{dg}) \right), \tag{22}$$

$$\dot{e}_{iqg} = \frac{di_{qg}^*}{dt} - \left(-b_1 i_{qg} - b_2 i_{dg} + b_3 v_{qi} \right). \tag{23}$$

We extend the Lyapunov function in Eq. (16) to include the state variables e_{idg} and e_{iqg}:

$$V_{eg} = \frac{1}{2} (e_{U_{dc}^2}^2 + e_{i_{dg}}^2 + e_{i_{qg}}^2). \tag{24}$$

We use V_{eg} to derive the control algorithm. To this end, we compute the derivative of V_{eg} along the error in Eqs. (22), (23), and (24):

$$\dot{V}_{eg} = e_{U_{dc}^2} \dot{e}_{U_{dc}^2} + e_{i_{dg}} \dot{e}_{i_{dg}} + e_{i_{qg}} \dot{e}_{i_{qg}}. \tag{25}$$

From the above, we can obtain the control laws as:

$$v_{di} = \frac{1}{b_3} \left(\frac{di_{dg}^*}{dt} - (-b_1 i_{dg} + b_2 i_{qg} - b_3 v_{dg}) + \frac{3}{C} v_{dg} e_{U_{dc}^2} + k_{i_{dg}} e_{i_{dg}} \right), \tag{26}$$

$$v_{qi} = \frac{1}{b_3} \left(\frac{di_{qg}^*}{dt} - (-b_1 i_{qg} - b_2 i_{dg}) + k_{i_{qg}} e_{i_{qg}} \right). \tag{27}$$

This leads to:

$$\dot{V}_e = -k_{U_{dc}^2} e_{U_{dc}^2}^2 - k_{i_{dg}} e_{i_{dg}}^2 - k_{i_{qg}} e_{i_{qg}}^2 \leq 0. \tag{28}$$

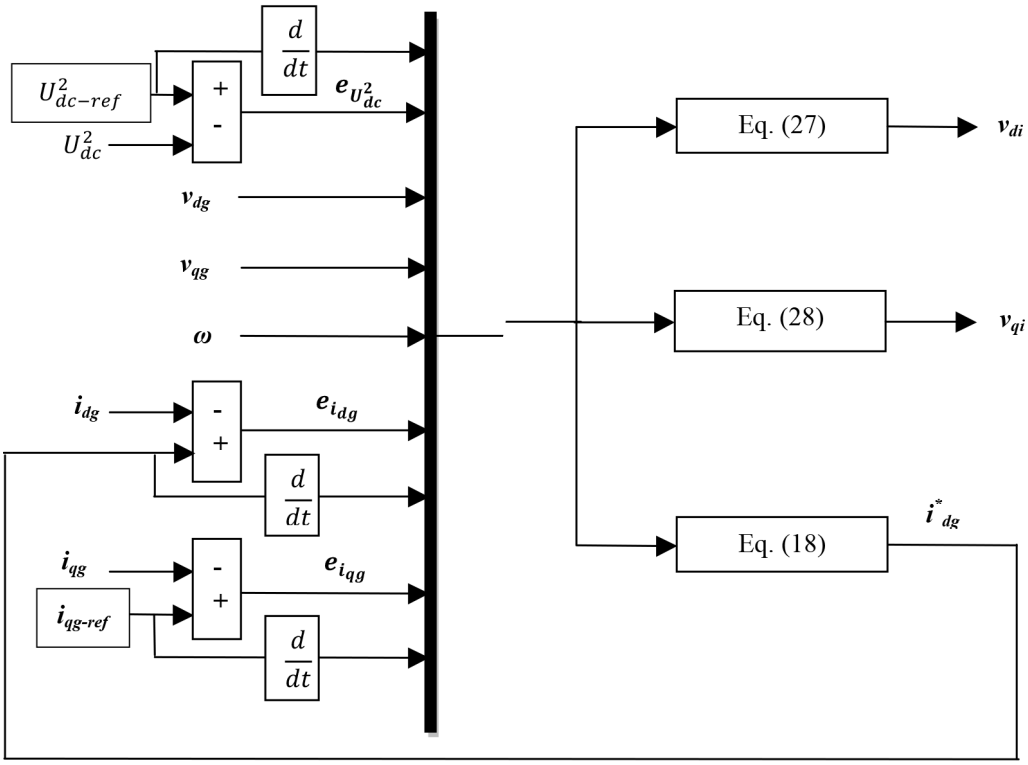

Figure 4. Simulink simulation model of the NBC with the input and output.

Proposition Using Lasalle's principle [15], the globally asymptotic stability of the system defined by Eqs. (11), (12), and (13) is guaranteed if the control laws are given by Eqs. (27) and (28), respectively.

4. Simulation system

The controllers of the DC-link voltage and PFC are implemented by Eq. (27) and (28) in a MATLAB/Simulink environment, as shown in Figure 4. The user can thereby use the controllers more efficiently and can establish the necessary settings easily.

Wind power is affected by the wind. The profile of the wind velocity imposed is shown in Figure 5, where v_n is a nominal value, and at this value, the WT-SCIG system produces nominal power (300 kW in our study).

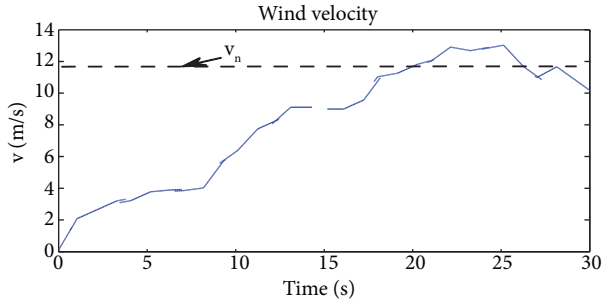

Figure 5. Wind velocity.

The simulated system is shown in Figure 1. The 3-MW wind farm is connected to a distribution system through 1-km transmission lines.

The system includes 10 SCIGs of 300 kW, driven by WTs through gearboxes. Such a system includes a pitch control, a VSC, a VSI, a filter, and controllers. During the simulation test, the DC-link voltage reference is fixed at 760 V and the reactive power reference is kept at 0 VAr. The parameters of the turbine and SCIG used are given in the Appendix, respectively, in Tables 1 and 2. Figure 6 shows the responses of the system for a change of the wind velocity. In order to prove the performances of the proposed nonlinear strategy, comparative simulation studies between this nonlinear controller (see Figure 6a) and the conventional scheme control using PI controllers (see Figure 6b) are carried out. The well-known pole placement method is used to determine the different PI controllers' gains. The PWM used in the system's inverter has a 5-kHz switching frequency for both methods of control. The distribution system frequency value is steady at 50 Hz.

The transient operation characteristics of the SCIG-wind farm are studied and compared with the NBC and PI controllers. The fault event is a 3-phase to ground short-circuit fault at bus 2 of the 2-MW loads, which begins at 25 s. After 200 ms, the fault is cleared. Figure 7 shows the transition performance of the grid-connected SCIG wind farm voltage control, with the NBC in Figure 7a and the PI controllers in Figure 7b.

5. Discussion and result analysis

The simulation results are shown in Figure 6a for the NBCs and Figure 6b for the conventional scheme with PI controllers. Figures 6a and 6b present the results of the simulation comparisons and, as desired, the DC-bus voltage is perfectly and quickly tracked to its input reference (U_{dc-ref} = 760 V). By comparing Figures 6a and 6b, it can be seen that the nonlinear approach offers a faster DC-link voltage than the conventional PI control method and this quantity is perfectly tracked to its input reference. It is also clear that the adopted control should guarantee that the active power and 3-phase current actual values should possess the ability of tracking their references as closely as possible, and it is clear that the active power component is proportional to the wind velocity. When the produced energy is greater than the nominal value, the generator speed is fixed to the upper limit and the pitch control is active to maintain the rated power (see at t = 21 s to t = 25 s). In spite of the wind velocity variation effects, these disturbances are instantaneously rejected and the control performances are not affected, whereas the response of the classical control is largely dependent on the currents and DC-link PI controller's parameters. As can be seen, this strategy is capable of providing accurate tracking for the reactive power reference and, meanwhile, keeping good decoupling of the active and reactive powers regulations. This implies that the wind farm supplies the distribution network with a purely active power. However, the PFC value of the wind farm is independent of the variation of the wind, but only on the reactive power reference. We confirm this by observing the phase voltage and current, where the reactive power oscillates at around 0. As can be deduced from the THD analysis, the NBC has a less harmonic and a clean sinus wave. When the THD values are compared, the controllers have values in the standard ranges; the THD of the NBC is 0.43% and the THD of the PI controller is 0.91%. However, the NBC's value is better than the PI's, as is its sinus wave form. Figure 7 shows the responses of the system during the fault period. Figure 7a presents the response of the proposed NBC, while Figure 7b gives the simulation results of the PI controllers. As can be seen, the NBC response presents better results than the system using PI controllers.

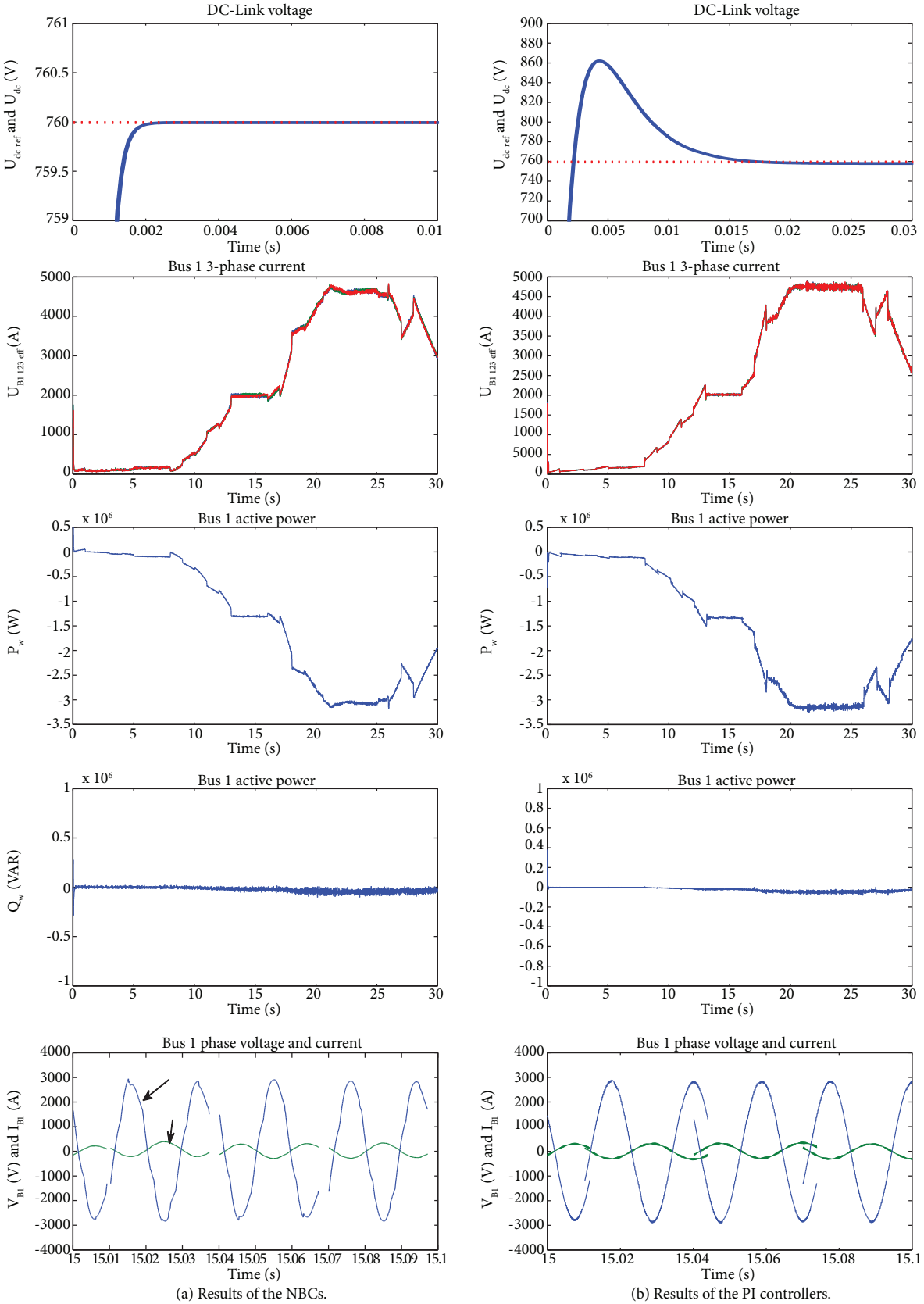

(a) Results of the NBCs.

(b) Results of the PI controllers.

Figure 6. Comparison results of the NBCs and PI controllers.

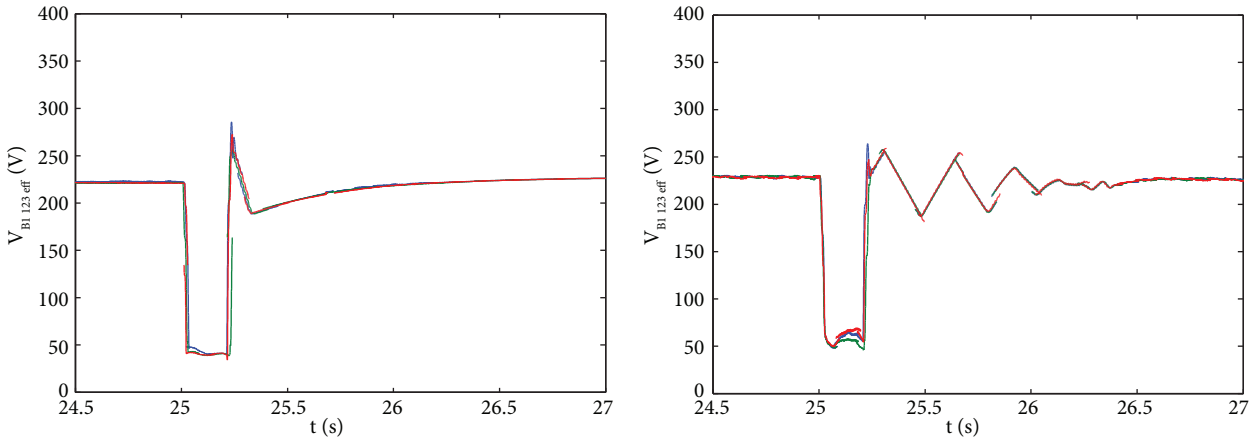

(a) Result of the NBCs.

(b) Result of the PI controllers.

Figure 7. Transition performance of the grid-connected SCIG wind farm voltage.

6. Conclusion

The paper presents a new control strategy of the wind power-connected distribution network. The resulting controllers proved to have good characteristics at different operating conditions, as was verified in the presented results. Both the DC-link voltage and the output active power were controlled to enhance the dynamic performance of the studied system. Comparisons between the system with PI controllers and the system with NBCs showed some differences between the 2 approaches. The following positive and advantageous aspects with the NBCs can be noted: the transient regime presents a faster system response, reaching the steady-state condition in shorter time. Thus, it is demonstrated that the SCIG's control voltage can be obtained using NBCs; these are a strong alternative to linear controllers and can be substituted with the referred advantages. It can be concluded from the simulation results of the wind farm set with the proposed NBC that:

- The proposed controller is much faster than the conventional PI controller and the DC-link voltage can be maintained at a constant value.
- It has excellent PFC control.
- The NBC has a less harmonic and a clean sinus wave.
- Good power quality of the power is forwarded to the distribution network.

Appendix: Parameters of the turbine-generator

Table 1. Parameters of the turbine.

Item	Symbol	Value
Air density	ρ	1.22 kg/m^3
Area swept by the blades	A	615.8 m^2
Speed-up gear ratio	G	23
Base wind speed	v_n	12 m/s
Turbine inertia	J_t	50 kg m^2

Table 2. Parameters of the SCIG.

Item	Symbol	Value
Rated power	P_n	300 kW
No. of poles	p	2
Rated speed	ω_n	158.7 rad/s
Stator resistance	R_s	0.0063 Ω
Stator inductance	L_s	0.0118 H
Mutual inductance	L_m	0.0116 H
Rotor resistance	R_r	0.0048 Ω
Rotor inductance	L_r	0.0116 H
Generator inertia	J_g	10 kg m^2

References

[1] C. Chompoo Inwai, W.J. Lee, P. Fuangfoo, M. Williams, J.R. Liao, "System impact study for the interconnection of wind generation and utility system", IEEE Transaction on Industry Applications, Vol. 41, pp. 163–168, 2005.

[2] O.Ö. Mengi, İ.H. Atlas, "Fuzzy logic control for a wind/battery renewable energy production system", Turkish Journal of Electrical Engineering & Computer Sciences, Vol. 20, pp. 187–206, 2012.

[3] M. Kesraoui, N. Korichi, A. Belkadi, "Maximum power point tracker of wind energy conversion system", Journal of Renewable Energy, Vol. 25, pp. 181–190, 2010.

[4] L.G. Gonzalez, E. Figueres, G. Garcere, O. Carranza, "Maximum-power-point tracking with reduced mechanical stress applied to wind-energy-conversion-systems", Journal of Applied Energy, Vol. 87, pp. 2304–2312, 2010.

[5] M. Benchagra, M. Maaroufi, M. Ouassaid, "Modeling and control of SCIG based variable-speed with power factor control", International Review of Modelling and Simulation, Vol. 4, pp. 1007–1014, 2011.

[6] T. Senjyu, Y. Ochi, Y. Kikunaga, M. Tokudome, A. Yona, E.B. Muhando, N. Urasaki, T. Funabashi, "Sensor-less maximum power point tracking control for wind generation system with squirrel cage induction generator", Journal of Renewable Energy, Vol. 34, pp. 994–999, 2009.

[7] E.J. Bueno, S. Cobreces, F.J. Rodrigues, A. Hernandez, F. Espinosa, "Design of back-to-back NPC converter interface for wind turbines with squirrel cage induction generator", IEEE Transactions on Energy Conversion, Vol. 23, pp. 932–945, 2008.

[8] L. Wang, J.H. Liu, "Dynamic analysis of a grid-connected marine current power generation system connected to a distribution system", IEEE Transaction on Power Systems, Vol. 25, pp. 1798–1805, 2010.

[9] Y. Oğuz, İ. Güney, "Adaptive neuro-fuzzy inference system to improve the power quality of variable-speed wind power generation system", Turkish Journal of Electrical Engineering & Computer Sciences, Vol. 18, pp. 625–646, 2010.

[10] A. Meharrar, M. Tioursi, M. Hatti, A.B. Stambouli, "A variable speed wind generator maximum power tracking based on adaptive neuro-fuzzy inference system", Journal of Expert Systems with Application, Vol. 38, pp. 7659–7664, 2011.

[11] X. Zheng, L. Li, D. Xu, J. Platts, "Sliding mode MPPT control of variable speed wind power system", Asia-Pacific Power and Energy Engineering Conference, pp. 1–4, 2009.

[12] M. Pahlevaninezhad, A. Safaee, S. Eren, A. Bakhshai, P. Jain, "Adaptive nonlinear maximum power point tracker for a WECS based on permanent magnet synchronous generator fed by a matrix converter", Energy Conversion Congress and Exposition, pp. 2578–2583, 2009.

[13] M. Benchagra, M. Maaroufi, M. Ouassaid, "Nonlinear MPPT control of squirrel cage induction generator-wind turbine", Journal of Theoretical and Applied Information Technology, Vol. 35, pp. 26–33, 2012.

[14] R. Penta, J.C. Clare, G.M. Asher, "Doubly fed induction generator using back-to-back PWM converters and its application to variable speed wind-energy generation", IEE Proceedings - Electric Power Applications, pp. 231–241, 1996.

[15] M. Krstic, I. Kanellakopoulos, P. Kokotovic, Nonlinear and Adaptive Control Design, New York, Wiley, 1995.